Dyes and Pigments 95 (2012) 96–101

Contents lists available at SciVerse ScienceDirect

Dyes and Pigments

journal homepage: www.elsevier.com/locate/dyepig

The effect of iron ions on the anatase–rutile phase transformation of titania (TiO_2) in mica–titania pigments

Qiang Gao [a,b], Xiaomei Wu [a,b,*], Yueming Fan [a,b]

[a] School of Materials Science and Engineering, South China University of Technology, Guangzhou 510641, People's Republic of China
[b] Key Laboratory of Specially Functional Materials of the Ministry of Education, South China University of Technology, Guangzhou 510641, People's Republic of China

ARTICLE INFO

Article history:
Received 8 October 2011
Received in revised form
13 March 2012
Accepted 28 March 2012
Available online 5 April 2012

Keywords:
Pearlescent pigment
Anatase–rutile transformation
Iron ions
TiO_2
Photocatalytic
Mica

ABSTRACT

Rutile TiO_2-coated mica–titania pigments were prepared by hydrolysis of titanium tetrachloride in the presence of Fe^{3+}. After calcination at 700 °C for 2 h, TiO_2 nanolayers in rutile phase were formed on the mica surfaces. The morphology and the anatase–rutile transformation were probed by scanning electronic microscopy (SEM) and X-ray diffraction (XRD) respectively. SEM micrographs show that the dopants enhance the growth of particles of TiO_2 thin layers. The change of lattice parameters confirms that Fe^{3+} enter anatase structure and affect the anatase–rutile transformation. For the iron loading regime studied here, the anatase–rutile transformation is inhibited at low dopant levels with respect to undoped titania. While the anatase–rutile transformation is promoted as iron loading is increased. Moreover, synthesized pH value also has a pronounced effect on the anatase–rutile transformation and a highly acidic environment favors the formation of rutile.

1. Introduction

Effect pigments have lustrous, iridescent and angle-dependent optical effects. These pigments are widely applied for functional and decorative purposes, such as optical filters, cosmetics, plastics, printed products, industrial coatings, and car paints for their effects [1–4]. The best known examples are the pearlescent pigments that are based on TiO_2 precipitated onto platelets of mica [5].

There are several approaches for synthesizing mica–titania pigments, such as sol–gel technique, chemical vapor deposition, and the hydrolysis of titanium tetrachloride [6–8]. Calcinations at 800 °C–900 °C convert the amorphous TiO_2 precipitate to crystalline TiO_2 thin layer [9]. Moreover, due to the anatase directing effect of mica [10], anatase and rutile still coexist when the calcination temperature is increased to 1000 °C [11]. It is well known that TiO_2 is a polymorphous compound, crystallizing as: rutile, anatase, or brookite. All of them have the same fundamental structural octahedral units with different arrangements [12]. In contrast with the other two phases, rutile TiO_2 is the most stable phase even in strongly acidic or basic conditions [13]. The refractive index of rutile (2.93) is higher than that of anatase (2.49), so that the effect of strong color and luster can be achieved when mica–titania pigments consist of complete rutile layers [11]. Furthermore, rutile has been found to show poor photocatalytic activities in most case [14,15], which may help to solve the problem of 'chalking' (photooxidation of surrounding polymeric binders in outdoor weathering initiated by the pigment) that has been besetting the coatings industry [16–18]. For above reasons, rutile modification of titanium dioxide in a pearlescent pigment is more desirable than the anatase modification.

Many researches [18–21] have focused on the phase transition behavior and photocatalytic activities of Fe^{3+}-doped TiO_2 nanoparticles. However, very few studies on the anatase–rutile transformation with the effect of iron ions for mica–titania pigments have been reported. In this study, mica–titania pigments were synthesized by hydrolysis of titanium tetrachloride and the effect of iron ions on the anatase–rutile transformation was investigated.

2. Experimental

2.1. Materials

The mica used as the substrate in this study was synthetic mica, supplied by Sanbao Pearl Luster Mica Tech CO., LTD, China. Dry mica flakes were sieved to obtain narrow size distribution. The SEM image of the naked mica shows that the mica powder has a flaky

* Corresponding author. School of Materials Science and Engineering, South China University of Technology, Guangzhou 510641, People's Republic of China. Tel./fax: +86 020 87114243.
E-mail address: imxmeiwu@scut.edu.cn (X. Wu).

0143-7208/$ – see front matter © 2012 Elsevier Ltd. All rights reserved.
doi:10.1016/j.dyepig.2012.03.030

shape with a fairly smooth surface (Fig. 1). These particles were of 10–70 μm in length and less than 1 μm in thickness.

Analytical grade titanium tetrachloride ($TiCl_4$), iron trichloride ($FeCl_3$), absolute ethanol (C_2H_5OH), sodium hydroxide (NaOH), and hydrochloric acid (HCl) were used in the experiments, throughout which distilled water was used.

The starting material in this study to deposit TiO_2 layer on mica was a mixed solution of titanium tetrachloride and absolute ethanol. In general, concentrated $TiCl_4$ gives a sudden reaction with water at room temperature, and $Ti(OH)_4$ forms [22]. In order to prevent such formation, $TiCl_4$ was added dropwise into absolute ethanol to obtain the precursor, the green clear mixed solution of titanium tetrachloride and absolute ethanol.

2.2. Preparation method

2.2.1. Preparation of undoped mica–titania pigments

The preparation of undoped mica–titania pigments was carried out in the following way [11,23]. First, 10 g of mica was dispersed with 1000 ml distilled water. The batch was then heated to 70 °C under stirring and the pH value was adjusted to 1.0 with diluted hydrochloric acid. Then 120 ml precursor was introduced into the agitated slurry at a constant speed of 0.5 ml/min. The pH value of the slurry was kept constant by simultaneous addition of NaOH solution. After the addition was completed, the slurry was aged for 1 h and then allowed to settle and cool to room temperature. Lastly, the particles were separated, washed with distilled water, and dried at 70 °C for 24 h. The final product was calcined at 800 °C for 2 h. This sample was labeled as TiO_2/M.

2.2.2. Preparation of doped mica–titania pigments

The introduction of Fe^{3+} in order to investigate the effect of iron ions on the anatase–rutile (A–R) transformation of TiO_2 thin layers was done by using $FeCl_3$ solution. First, mica was suspended in distilled water and heated to 70 °C, and then pH value was adjusted to 2.0 by using HCl. Then, $FeCl_3$ aqueous solution (15 g/l) was added dropwise while pH value was held constant by simultaneous addition of NaOH solution for 1 h. The weight rations of $FeCl_3$ to mica were 1%, 2%, 3% and 4% respectively. Then, pH value was adjusted to 1.0, and the TiO_2 coating was deposited on mica by addition of precursor the same way as described in 2.2.1. After drying, the products were calcined for 2 h at various temperatures (200, 400, 600, 700, and 800 °C).

In order to investigate the effect of pH value on the anatase–rutile (A–R) transformation, the weight rations of $FeCl_3$ to mica was fixed at 3%, and the pH value of the slurry during the introduction of precursor was adjusted to 1, 3, 5, 7 and 9 respectively. And the products were calcined at 800 °C for 2 h.

2.3. Characterization

2.3.1. X-ray diffraction analysis

X-ray powder diffraction (XRD) analysis was done on a PANalytical X'Pert Pro diffractometer using Cu Kα radiation at 40 kV and 40 mA for the crystal structure determination of TiO_2 on mica. XRD patterns were recorded in the 2θ range from 20° to 60° with a step size of 0.01° and a scan step time of 0.3 s.

The percentages of anatase and rutile in TiO_2 layer were calculated from X-ray powder diffraction intensities corresponding to anatase (101) and rutile (110) reflections. Then, the mass fraction of rutile, X_R, was determined by following equation [24,25].

$$X_R = \frac{1}{1 + 1.26(I_A/I_R)} \times 100\% \quad (1)$$

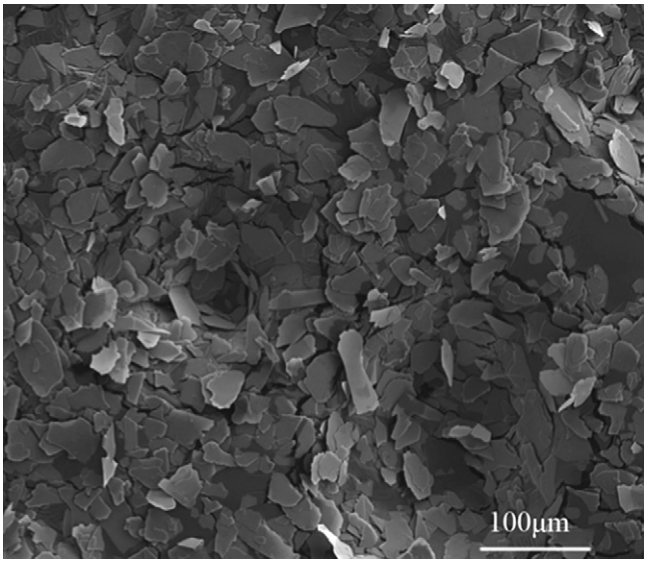

Fig. 1. SEM image of mica particles.

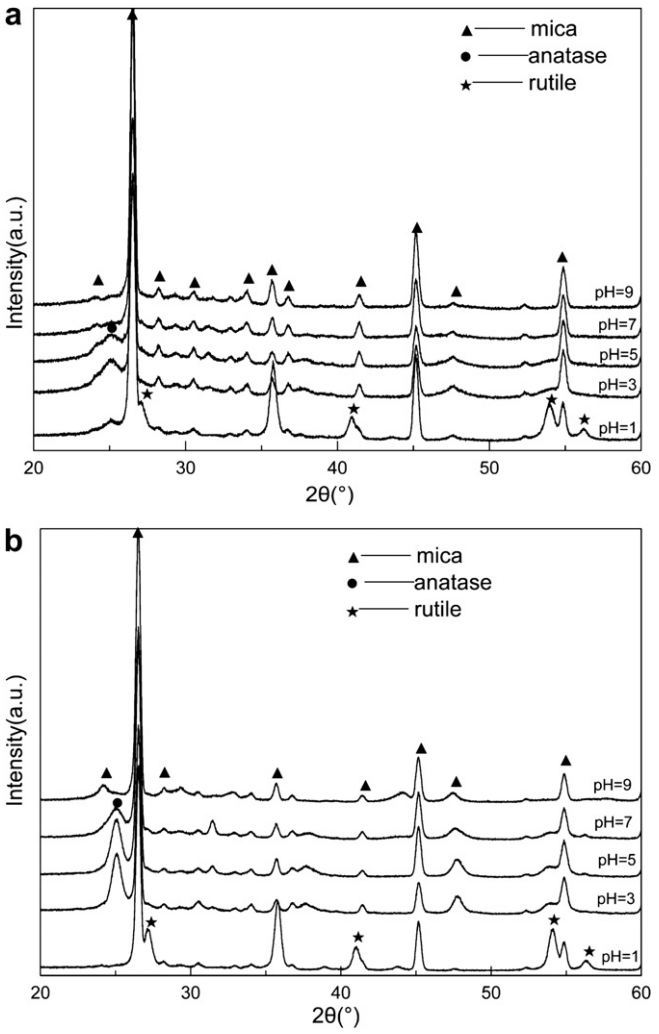

Fig. 2. X-ray diffraction patterns of iron-doped mica–titania pigments with various synthesized pH values of 1, 3, 5, 7, and 9, respectively. (a) The samples were dried at 70 °C for 24 h; (b) The samples were calcined at 800 °C for 2 h.

where I_A and I_R are the intensities of anatase (101) reflection and rutile (110) refection, respectively.

2.3.2. Scanning electronic microscopy analysis

The samples were examined by scanning electron microscopy (SEM, Nova NanoSEM 430, FEI Company) to characterize the morphological changes associated with the doping of iron ions. The operation voltage was 10 kV.

2.3.3. FTIR spectra analysis

FTIR spectra for samples were measured by Bruker Vector 33 spectrometer in a region of 400–4000 cm^{-1}.

3. Results and discussion

3.1. The effect of pH value on the anatase–rutile (A–R) transformation

The X-ray diffraction patterns of iron ions doped mica–titania pigments prepared at different pH values are shown in Fig. 2. The XRD peaks appearing at $2\theta = 25.1°$ is that of anatase TiO_2 (JCPDS 21-1272). And the XRD peaks appearing at $2\theta = 27.1$, 40.9, 54.0, 56.2° are that of rutile TiO_2 (JCPDS 21-1276). It is found that when the synthesized pH value is as low as 1, in addition to anatase, there is also rutile. Only the peak of anatase phase appears with increasing pH values. And when the synthesized pH value is increased to 7, there are no peaks of TiO_2, which indicates that TiO_2 may exist in amorphous form (Fig. 2a). It is obvious that all the peaks of anatase and rutile are broad and weak without calcination. After calcination, anatase phase appears for the sample synthesized at pH value of 7 but no peaks of TiO_2 for the sample synthesized at pH value of 9 (Fig. 2b). It is observed from Fig. 2 that the formation of rutile is dependent on pH value, and a highly acidic medium favors the formation of rutile.

In order to study whether hydroxide exists in the samples prepared at different pH values without calcination, FTIR spectroscopy analysis was done. Several bands corresponding to hydroxyls in the samples are observed in Fig. 3. It can be seen that the deformation vibrations of adsorbed water molecules (1600–1700 cm^{-1}) and stretching vibrations of hydroxyl groups (3100–3500 cm^{-1}) [26–28]. These hydroxide groups in Ti–OH form the TiO_2 nanocrystals by condensation reaction at elevated temperature. So when the synthesized pH value is as low as 1, in addition to anatase and rutile, titanium hydroxylate may also exist.

In general, anatase–rutile transformation requires a fairly high temperature, varying from 400 to 1200 °C in a solid-state reaction [29,30]. So it is unusual to observe the transformation of anatase to rutile at the low temperature of 70 °C. And there must be a different mechanism involved in the low temperature transformation. Since rutile is the thermodynamically stable phase, the formation of rutile probably takes place through a dissolution-crystallization mechanism [31]. First, anatase would form by the hydrolysis of $TiCl_4$, but this anatase is not stable and highly distorted in strong acid environment. Then, the anatase dissolves to form titanium hydroxylate, an unstable intermediate. Lastly, the precipitations of titanium hydroxylate form rutile.

3.2. The effect of temperature on the anatase–rutile (A–R) transformation

Fig. 4 shows that the intensity of rutile increases and the peaks of rutile sharpen with increasing calcination temperature while the intensity of anatase decreases. When the calcination temperature is increased to 700 °C, the TiO_2 in the mica–titania pigments is in rutile form, so anatase is transformed completely to rutile. Fig. 5 shows the graphical illustration of the change of mass fraction of rutile phase with varying calcination temperature. It is observed that the mass fraction of rutile phase increases with the increasing temperatures and finally reaches 100%.

3.3. The effect of dopant loading on the anatase–rutile (A–R) transformation

Fig. 6 shows that the intensity of anatase increases sharply after doping with respect to undoped titania. Then the intensity of rutile increases and the peaks of rutile sharpen with increasing dopant loadings while the intensity of anatase decreases. When the dopant loading is increased to 3%, the TiO_2 in the mica–titania pigments is in rutile phase, so anatase transforms to rutile completely.

Fig. 7 shows the graphical illustration of the change of mass fraction of rutile phase with varying dopant levels. It is clear that the mass fraction of rutile phase drops firstly and then goes up

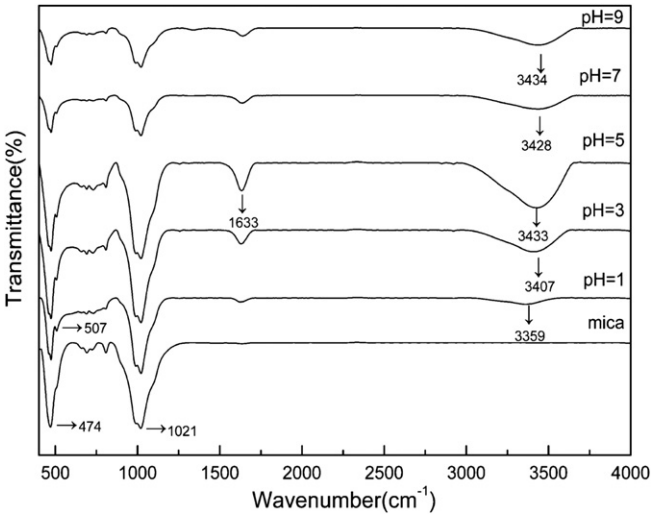

Fig. 3. A set of FTIR spectra of iron-doped mica–titania pigments with various synthesized pH values of 1, 3, 5, 7, and 9, respectively. The samples were dried at 70 °C for 24 h.

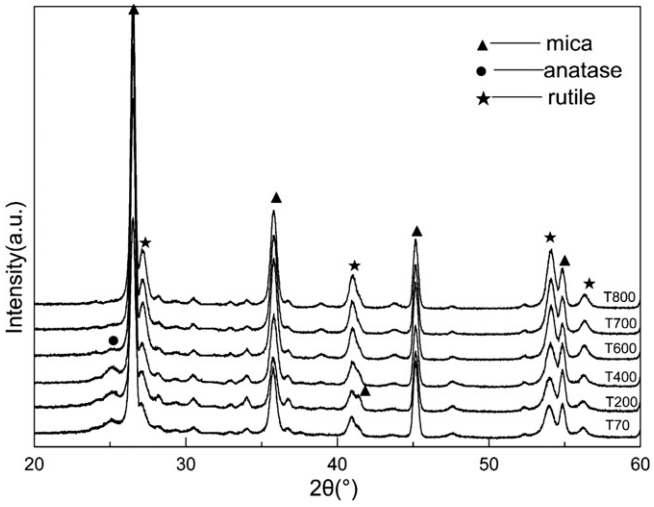

Fig. 4. X-ray diffraction patterns obtained for the iron-doped mica–titania pigments calcined at different temperatures: 70, 200, 400, 600, 700, 800 °C. The weight ration of $FeCl_3$ to mica was 3%.

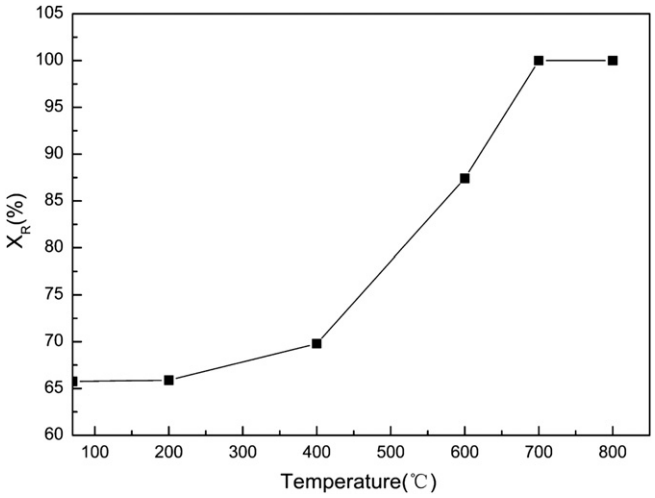

Fig. 5. Mass fraction of rutile phase of the iron-doped mica–titania pigments calcined at different temperatures. The weight ration of $FeCl_3$ to mica was 3%.

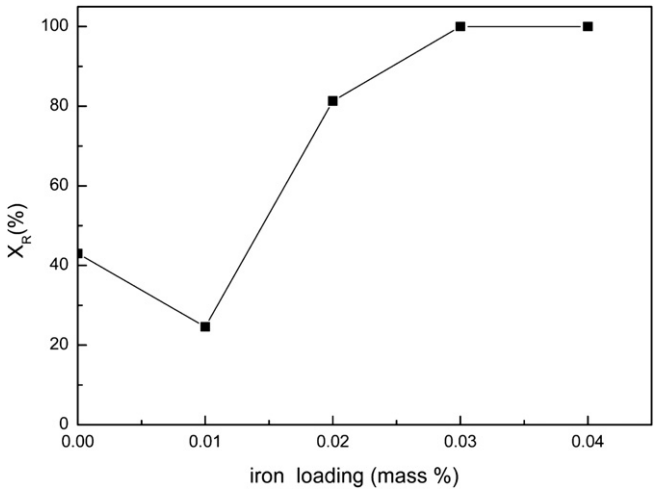

Fig. 7. Mass fraction of rutile phase of the iron-doped mica–titania pigments with different dopant loadings.

gradually with increasing dopant loadings, which is followed by a leveling off at 100%.

Fig. 8 shows SEM images of the morphology of TiO_2 thin layers deposited on mica. The surface of TiO_2 thin layers on mica appears to be smooth and uniform. However, particle size of TiO_2 thin layers becomes larger after doping. The average particle size of TiO_2 thin layers for undoped sample and the iron doped sample with the dopant level of 3% is about 27 and 55 nm, respectively. This explains why the first one looks denser than the second one and shows that iron ions enhance the growth of particles of TiO_2 thin layers.

In order to know how iron ions affect the anatase–rutile transformation of TiO_2, crystal structures of the phases can be examined (Table 1). It can be seen that the lattice parameters and $d_{(110)}$ of rutile phase do not change significantly after doping. But the lattice parameters increases after doping and $d_{(101)}$ increases with the increasing dopant loadings for the anatase phase. And the ion radius of Ti^{4+} and Fe^{3+} are 0.061, 0.064 nm respectively [11]. This indicates that Fe^{3+} ions enter anatase structure and affect anatase–rutile transformation. When iron loading is at low dopant levels, Fe^{3+} ion may enter the interstitial positions in the anatase

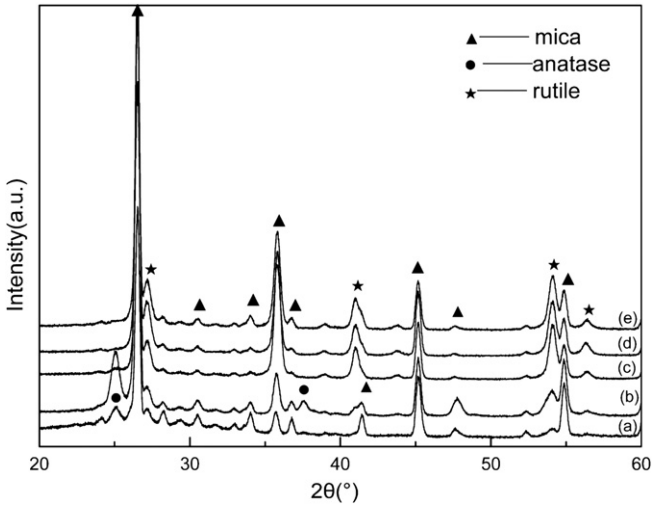

Fig. 6. XRD patterns of mica–titania pigments with different iron doping loadings: (a) 0, (b) 1%, (c) 2%, (d) 3%, (e) 4%.

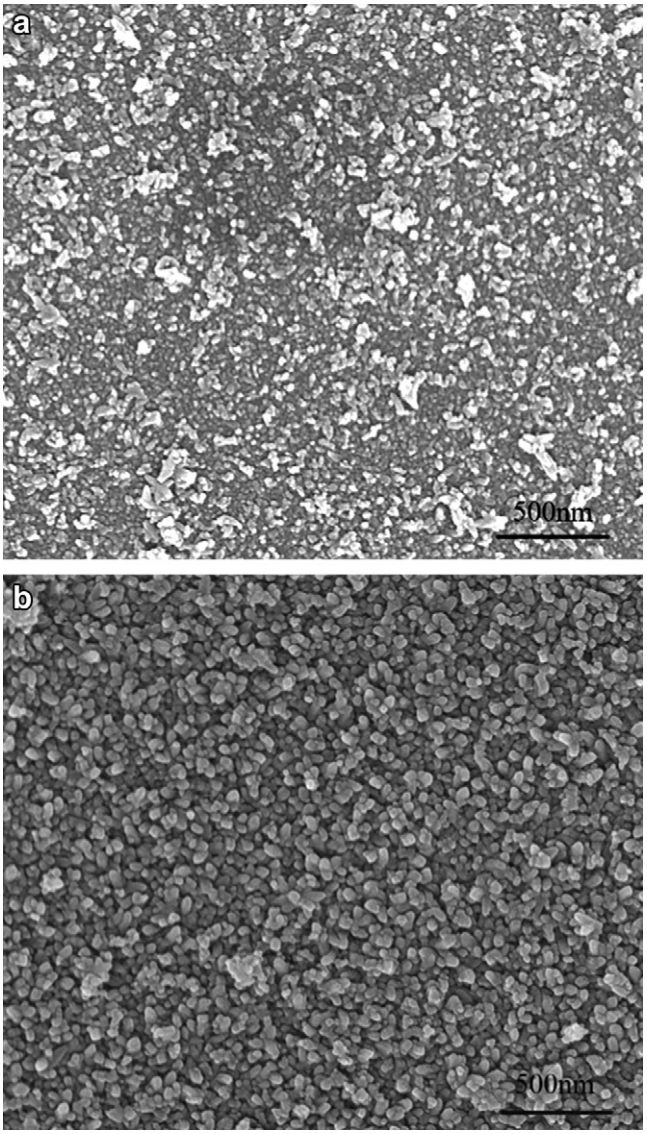

Fig. 8. SEM micrographs of mica–titanium pigments calcinated at 800 °C for 2 h :(a) TiO_2/mica, (b) 3% iron-doped mica–titania pigments.

Table 1
The lattice parameters and $d_{(hkl)}$ value of TiO_2 in the pure and doped mica–titanium samples annealed at 800 °C for 2 h. F0.01, F0.02, F0.03, F0.04 are the doped samples with the dopant loading of 1%, 2%, 3% and 4% respectively. The unit of all the values is angstrom (Å).

Sample label	Anatase phase			Rutile phase		
	a	c	$d_{(101)}$	a	c	$d_{(110)}$
TiO_2/M	3.7986	9.4914	3.5454	4.6164	2.9844	3.2776
F0.01	3.8030	9.5600	3.5598	4.6164	2.9870	3.2859
F0.02	–	–[a]	3.5620	4.6137	2.9835	3.2718
F0.03				4.6127	2.9881	3.2730
F0.04				4.6122	2.9867	3.2713

[a] Could not calculated because of the low intensity of peaks.

lattice. Arroyo et al. [32] and Janes et al. [18] have argued that interstitial occupancy would reduce oxygen deficiency and retard the anatase–rutile transformation rate. This explains the decline of mass fraction of rutile phase for the iron doped sample with the dopant loading of 1% with respect to the undoped sample. As the iron loading is increased, it is probably that Ti^{4+} is substituted by Fe^{3+} ion as following equation:

$$Fe_2O_3 \xrightarrow{TiO_2} 2Fe_{Ti'} + V_{O^{\cdot}} + 3O_O \quad (2)$$

Substitutional incorporation of Fe^{3+} would generate oxygen vacancies on simple charge compensation grounds. Gouma suggested that the anatase–rutile transformation involve the break of Ti–O bonds and a cooperative movement of the Ti and O atoms [33]. And oxygen vacancies can offer space for the atomic arrangement. So Fe^{3+} ion can promote anatase–rutile transformation. What's more, Hu et al. [34] and Reidy et al. [35] suggested that the beginning of anatase–rutile transformation depends on the growth rate of anatase particles to attain the critical size. And oxygen vacancies favor the mass transport requirement of reaching the critical particle size. So the generation of oxygen vacancies can promote the anatase–rutile transformation. Besides, oxygen vacancies increase with the increasement of dopant loading, so the mass fraction of rutile phase increases with the increasing dopant loading.

4. Conclusions

Nanometer titanium dioxide (TiO_2) was deposited on mica flakes by using a chemical liquid deposition method. Use of only 3 wt% $FeCl_3$ with respect to mica weight was found to begin to provide a complete rutile TiO_2 coating after calcination at 700 °C for 2 h. The morphology and the anatase–rutile transformation were studied by SEM and X-ray diffraction analysis. SEM showed that the particle size of TiO_2 thin layers became larger after doping. The X-ray diffraction analysis proved that the dopant had a pronounced effect on the anatase–rutile transformation. The anatase–rutile transformation was inhibited at low dopant levels with respect to undoped titania. But the anatase–rutile transformation was promoted as iron loading was increased. The change of lattice parameters confirmed that Fe^{3+} entered anatase structure and affected the anatase–rutile transformation. Moreover, synthesized pH value also had a pronounced effect on the anatase–rutile transformation and a highly acidic environment favored the formation of rutile.

Acknowledgments

The authors thank Huazhi Su, Shaohua Wang and Chuxin Zhang very much for kindly supporting the X-ray diffraction measurement of the samples. We also thank Dr Song (Analytical and Testing Center, South China University of Technology) for FTIR. The work was funded by the Key Laboratory of Specially Functional Materials, South China University of Technology, Ministry of Education, China.

References

[1] Maile FJ, Pfaff G, Reynders P. Effect pigments – past, present and future. Progress in Organic Coatings 2005;54(3):150–63.
[2] Kirchner E, Houweling J. Measuring flake orientation for metallic coatings. Progress in Organic Coatings 2009;64(2–3):287–93.
[3] Tan JR, Fu XS, Hou WX, Chen XZ, Wang L. The preparation and characteristics of a multi-cover-layer type, blue mica titania, pearlescent pigment. Dyes Pigments 2003;56(2):93–8.
[4] Stengl V, Subrt J, Bakardjieva S, Kalendova A, Kalenda P. The preparation and characteristics of pigments based on mica coated with metal oxides. Dyes Pigments 2003;58(3):239–44.
[5] Pfaff G, Reynders P. Angle-dependent optical effects deriving from submicron structures of films and pigments. Chemical Reviews 1999;99(7):1963–82.
[6] Hildenbrand VD, Doyle S, Fuess H, Pfaff G, Reynders P. Crystallisation of thin anatase coatings on muscovite. Thin Solid Films 1997;304(1–2):204–11.
[7] Bayat N, Baghshahi S, Alizadeh P. Synthesis of white pearlescent pigments using the surface response method of statistical analysis. Ceramics International 2008;34(8):2029–35.
[8] Cho JH, Lim SH. Internal structure analysis of mica particles coated with metal oxide by transmission electron microscopy. Dyes Pigments 2006;69(3):192–5.
[9] Cho JH, Tark YD, Kim WY, Lim SH. Room-temperature synthesis and characteristics of nanocrystalline TiO_2 on mica by homogeneous precipitation. Metals and Materials International 2009;15(6):1001–5.
[10] Deluca CV, Cerce LR, Deluca C, Cerce L, inventors. Engelhard Corporation, assignee. Rutile titanium dioxide effect pigments and production thereof. United States patent 6626989-B1; 2002 May 16.
[11] Song GB, Liang JK, Liu FS, Peng TJ, Rao GH. Preparation and phase transformation of anatase–rutile crystals in metal doped TiO_2/muscovite nanocomposites. Thin Solid Films 2005;491(1–2):110–6.
[12] Wang Y, Zhang L, Deng K, Chen X, Zou Z. Low temperature synthesis and photocatalytic activity of rutile TiO_2 nanorod superstructures. The Journal of Physical Chemistry C 2007;111(6):2709–14.
[13] Ge M, Li JW, Liu L, Zhou Z. Template-free synthesis and photocatalytic application of rutile TiO_2 hierarchical nanostructures. Industrial & Engineering Chemistry Research 2011;50(11):6681–7.
[14] Zhang S, Liu C-Y, Liu Y, Zhang Z-Y, Mao L-J. Room temperature synthesis of nearly monodisperse rodlike rutile TiO_2 nanocrystals. Materials Letters 2009;63(1):127–9.
[15] Lu A, Liu J, Zhao D, Guo Y, Li Q, Li N. Photocatalysis of V-bearing rutile on degradation of halohydrocarbons. Catalysis Today 2004;90(3–4):337–42.
[16] Allen NS, Edge M, Ortega A, Sandoval G, Liauw CM, Verran J, et al. Degradation and stabilisation of polymers and coatings: nano versus pigmentary titania particles. Polymer Degradation and Stability 2004;85(3):927–46.
[17] Allen NS, Edge M, Sandoval G, Ortega A, Liauw CM, Stratton J, et al. Interrelationship of spectroscopic properties with the thermal and photochemical behaviour of titanium dioxide pigments in metallocene polyethylene and alkyd based paint films: micron versus nanoparticles. Polymer Degradation and Stability 2002;76(2):305–19.
[18] Janes R, Knightley LJ, Harding CJ. Structural and spectroscopic studies of iron (III) doped titania powders prepared by sol–gel synthesis and hydrothermal processing. Dyes Pigments 2004;62(3):199–212.
[19] Wang JA, Limas-Ballesteros R, López T, Moreno A, Gómez R, Novaro O, et al. Quantitative determination of titanium lattice Defects and solid-state reaction mechanism in iron-doped TiO_2 Photocatalysts. The Journal of Physical Chemistry B 2001;105(40):9692–8.
[20] Gennari FC, Pasquevich DM. Kinetics of the anatase–rutile transformation in TiO_2 in the presence of Fe_2O_3. Journal of Materials Science 1998;33(6):1571–8.
[21] Lopez T, Moreno JA, Gomez R, Bokhimi X, Wang JA, Yee-Madeira H, et al. Characterization of iron-doped titania sol–gel materials. Journal of Materials Chemistry 2002;12(3):714–8.
[22] Topuz BB, Gündüz G, Mavis B, Çolak Ü. The effect of tin dioxide (SnO_2) on the anatase–rutile phase transformation of titania (TiO_2) in mica–titania pigments and their use in paint. Dyes Pigments 2011;90(2):123–8.
[23] Ryu YC, Kim TG, Seo GS, Park JH, Suh CS, Park SS, et al. Effect of substrate on the phase transformation of TiO_2 in pearlescent pigment. Journal of Industrial and Engineering Chemistry 2008;14(2):213–8.
[24] Gennari FC, Pasquevich DM. Enhancing effect of iron chlorides on the anatase–rutile transition in titanium dioxide. Journal of the American Ceramic Society 1999;82(7):1915–21.
[25] Spurr RA, Myers H. Quantitative analysis of anatase–rutile mixtures with an X-ray diffractometer. Analytical Chemistry 1957;29(5):760–2.
[26] Burgos M, Langlet M. The sol–gel transformation of TIPT coatings: a FTIR study. Thin Solid Films 1999;349(1–2):19–23.
[27] Lee L-H, Chen W-C. High-refractive-index thin films prepared from trialkoxysilane-capped poly(methyl methacrylate)–titania materials. Chemistry of Materials 2001;13(3):1137–42.

[28] Qian L, Du Z-L, Yang S-Y, Jin Z-S. Raman study of titania nanotube by soft chemical process. Journal of Molecular Structure 2005;749(1–3): 103–7.
[29] Jung HS, Shin H, Kim J-R, Kim JY, Hong KS, Lee J-K. In situ observation of the stability of anatase nanoparticles and their transformation to rutile in an acidic solution. Langmuir 2004;20(26):11732–7.
[30] Wallot J, Reynders P, Herzing AA, Kiely CJ, Harmer MP, Rödel J. Sintering of thin film nanocrystalline titania-tin oxide composites. Journal of the European Ceramic Society 2008;28(11):2225–32.
[31] Jolivet JP. Metal oxide chemistry and synthesis. John Willy and Sons; 2000.
[32] Arroyo R, Córdoba G, Padilla J, Lara VH. Influence of manganese ions on the anatase–rutile phase transition of TiO_2 prepared by the sol–gel process. Materials Letters 2002;54(5–6):397–402.
[33] Gouma PI, Mills MJ. Anatase-to-rutile transformation in titania powders. Journal of the American Ceramic Society 2001;84(3):619–22.
[34] Hu Y, Tsai HL, Huang CL. Phase transformation of precipitated TiO_2 nanoparticles. Materials Science and Engineering: A 2003;344(1–2):209–14.
[35] Reidy DJ, Holmes JD, Morris MA. The critical size mechanism for the anatase to rutile transformation in TiO_2 and doped-TiO_2. Journal of the European Ceramic Society 2006;26(9):1527–34.